Journal of Alloys and Compounds 388 (2005) 159–167

Journal of ALLOYS AND COMPOUNDS

www.elsevier.com/locate/jallcom

A comparative Mössbauer spectral study of the electronic and magnetic properties of $Nd_6Fe_{13}Ag$ and $Nd_6Fe_{13}AgH_{13}$

Dimitri Hautot[a], Gary J. Long[a,*], Fernande Grandjean[a,b], K.H.J. Buschow[c]

[a] *Department of Chemistry, University of Missouri-Rolla, Rolla, MO 65409-0010, USA*
[b] *Department of Physics, B5, University of Liège, B-4000 Sart-Tilman, Belgium*
[c] *Van der Waals-Zeeman Institute, University of Amsterdam, Valckenierstraat 65, NL-1018 XE Amsterdam, The Netherlands*

Received 4 July 2004; accepted 6 July 2004

Abstract

The Mössbauer spectra of $Nd_6Fe_{13}Ag$ and $Nd_6Fe_{13}AgH_{13}$ have been measured between 85 and 295 K and analyzed with a model that takes into account the basal magnetic anisotropy, the iron and hydrogen near-neighbor environments of the five crystallographically and magnetically inequivalent 4*d*, 16*k*, 16*k*′, 16l_1, and 16l_2 iron sites in the former and the six crystallographically and magnetically inequivalent 4*d*, 16*k*, 16*k*′, 16l_1, 16l_{2-1} and 16l_{2-2} iron sites in the latter, where the additional site results from a predominance of hydrogen as near-neighbors on the iron 16l_2 site. The increases in hyperfine field and isomer shift observed upon hydrogenation are in agreement with the increase in Wigner–Seitz cell volumes of each site and the changes in the near-neighbor environments.

Keywords: Hydrogen storage materials; Hard magnetic materials; Mössbauer spectroscopy; Hyperfine parameters

1. Introduction

During the extensive search for new magnetic materials for use in hard permanent magnet applications, a new ternary rare-earth-iron-metal phase, of general stoichiometry $R_6Fe_{13}X$, where R is typically a light rare-earth and X is a metal, such as copper, silver, or gold, or a metametal, such as silicon or germanium, was identified [1,2]. These compounds crystallize in the $Nd_6Fe_{13}Si$ structure [3,4], with the *I4/mcm* tetragonal space group, a structure which consists of successive *C*, *B*, A_1, *S*, A_2, *B*, *C*,... layers which are perpendicular to the tetragonal *c*-axis, layers that make up one-half of the unit cell of $R_6Fe_{13}X$. Layer *C* contains iron on the 4*d* and 16*k* crystallographic sites, layer *B* contains iron on the 16l_1 and 16l_2 sites and neodymium on the 8*f* site, layers A_1 and A_2 contain neodymium on the 16*l* site, and layer *S* contains X on the 4*a* site. Thus in $R_6Fe_{13}X$ iron occupies four crystallographically inequivalent sites, the 4*d*, 16*k*, 16l_1, and 16l_2 sites, with 12, 10, 9, and 7 iron near neighbors, respectively; surprisingly, the iron sites have no X near-neighbors.

The magnetic properties of $R_6Fe_{13}X$ with various X elements have been studied [3–9] and the properties of $Nd_6Fe_{13}Si$ have proven [3,8,10,11] to be unusually interesting because it exhibits a magnetic spin reorientation upon cooling below 110 K. Because of the spin reorientation observed in $Nd_6Fe_{13}Si$, it is essential to have a good understanding of the Mössbauer spectra of the various $Nd_6Fe_{13}X$ compounds. Fortunately, there have been several very useful earlier Mössbauer spectral studies of $Nd_6Fe_{13}X$ where X is Cu [6], Ag [4,9], Au [4,7], Ge [12], In [13], Tl [13], Sn [9,13] and Pb [13], studies which indicate that the spectra are very sensitive to both the local environments and the nature of the magnetic anisotropy, i.e., axial or basal.

Because Mössbauer spectra are also known [14–22] to be sensitive to the presence both of hydrogen and to any spin-reorientations found in intermetallic compounds, we have undertaken a detailed comparative Mössbauer spectral study

* Corresponding author. Tel.: +1-573-341-4438; fax: +1-573-341-6033.
E-mail addresses: glong@umr.edu (G.J. Long), fgrandjean@ulg.ac.be (F. Grandjean), buschow@science.uva.nl (K.H.J. Buschow).

0925-8388/$ – see front matter © 2004 Elsevier B.V. All rights reserved.
doi:10.1016/j.jallcom.2004.07.017

of the electronic and magnetic properties of $Nd_6Fe_{13}Ag$ and $Nd_6Fe_{13}AgH_{13}$, the results of which are reported herein.

2. Experimental

The sample of $Nd_6Fe_{13}Ag$ was prepared by arc melting starting materials of at least 99.9% purity and is the same sample as was used in earlier studies [7,8,10]. After arc melting the sample was wrapped in tantalum foil, sealed in an evacuated quartz tube, annealed for 4 weeks at 900 K, and quenched to room temperature. The X-ray powder diffraction pattern indicated that the annealed sample contained only $Nd_6Fe_{13}Ag$ which was crystallized in the tetragonal $Nd_6Fe_{13}Si$ structure [3].

The synthesis of the hydride of $Nd_6Fe_{13}Ag$ was carried out at pressures not exceeding 2 bar using hydrogen gas with a purity of 99.99%. The $Nd_6Fe_{13}Ag$ starting material was initially activated by annealing in a dynamic vacuum at 600 K for 30 min. After activation, the $Nd_6Fe_{13}Ag$ was cooled to room temperature and hydrogen was injected into the stainless steel autoclave. The hydrogenation began instantly and proceeded exothermically and rapidly until a nominal composition of $Nd_6Fe_{13}AgH_{13}$ was achieved, see below.

The X-ray diffraction pattern indicated that $Nd_6Fe_{13}AgH_{13}$ also crystallized in the tetragonal $Nd_6Fe_{13}Si$ structure with the lattice parameters given in Table 1. The absorption of hydrogen is accompanied by an expansion of the lattice by 14.43%, an expansion that is consistent with the absorption of 13 hydrogen atoms per formula unit of $Nd_6Fe_{13}Ag$ as is indicated by the very similar expansion observed for $Pr_6Fe_{13}Au$ when it forms $Pr_6Fe_{13}AuD_{13}$.

Table 1
Lattice parameter changes upon hydrogenation

Compound	*a* (Å)	*c* (Å)	*c*/*a*	*V* (Å^3)
$Nd_6Fe_{13}Ag$	8.0854 (2)	22.591 (1)	0.358	1476.86 (1)
$Nd_6Fe_{13}AgH_{13}$	8.177 (1)	25.275 (1)	0.324	1689.97 (4)
Increase	0.092 (1)	2.684 (1)	–	213.2 (4)
Increase (%)	1.13	11.88	–	14.43
$Pr_6Fe_{13}Au$	8.0962 (3)	22.672 (1)	0.357	1486.1 (2)
$Pr_6Fe_{13}AuD_{13}$	8.1735 (8)	25.408 (4)	0.322	1697.4 (5)
Increase	0.0773 (8)	2.736 (4)	–	211.2 (5)
Increase (%)	0.95	12.07	–	14.22

The Mössbauer spectra were obtained between 85 and 295 K on a constant acceleration spectrometer which utilized a room temperature rhodium matrix cobalt-57 source and was calibrated at room temperature with α-iron foil. The Mössbauer spectral absorbers, which contained 26–29 mg/cm^2 of compound, were prepared from pieces of samples pulverized under liquid toluene and sieved to particle diameters of approximately 0.045 mm or smaller. The accuracy of the hyperfine parameters obtained from Lorentzian line shape fits is estimated to be ±0.005 mm/s for the isomer shift, ±0.05 mm/s for the quadrupole shift, and ±0.2 T for the hyperfine field. Variations of the hyperfine parameters within these limits lead to minor but insignificant increases in MISFIT, [23] which is of the order of 0.5–0.8% for all fits reported herein.

3. Results and discussion

X-ray powder diffraction patterns indicate that both $Nd_6Fe_{13}Ag$ and $Nd_6Fe_{13}AgH_{13}$ crystallize with the tetragonal $Nd_6Fe_{13}Si$ structure in the *I*4/*mcm* space group. The lattice parameters are given in Table 1 where it may be noted that the lattice parameters of $Nd_6Fe_{13}AgH_{13}$ are almost identical to those of $Pr_6Fe_{13}AuD_{13}$. On the basis of this similarity it has been assumed herein that $Nd_6Fe_{13}Ag$ has been fully hydrogenated to form $Nd_6Fe_{13}AgH_{13}$.

Unfortunately, there has been no neutron diffraction study of the distribution of hydrogen in the lattice of $Nd_6Fe_{13}AgH_{13}$ and it will be assumed herein that this distribution is the same as that found [24] in $Pr_6Fe_{13}AuD_{13}$. Thus we have used the lattice parameters given in Table 1, along with the positional parameters reported [24] for $Pr_6Fe_{13}AuD_{13}$, to both calculate the Wigner–Seitz cell volume of each iron site in $Nd_6Fe_{13}AgH_{13}$ and to determine its number of near-neighbor hydrogen atoms, see Table 2.

The Mössbauer spectra of $Nd_6Fe_{13}Ag$ and $Nd_6Fe_{13}AgH_{13}$, obtained at several temperatures, are shown in Figs. 1 and 2. The hyperfine parameters for the fits shown in these figures are given in Tables 3 and 4. The hyperfine parameters for the 295 and 85 K spectra of $Nd_6Fe_{13}Ag$ have been reported earlier [10]. A simple visual comparison of the spectra of $Nd_6Fe_{13}Ag$ and $Nd_6Fe_{13}AgH_{13}$ obtained at 85 K reveals the dramatic influence the addition

Table 2
The near-neighbor hydrogen environments[a] and the Wigner–Seitz cell volumes of the iron sites in $Nd_6Fe_{13}AgH_{13}$

Parameter/site	H(1) 8*g*	H(2) 16*l*	H(3) 4*c*	H(4) 32*m*	H(5) 32*m*	H(6) 32*m*	Total number of *H*nn	V_{WS}[b] (Å^3)
H occupancy	0.775	0.706	1.000	0.715	0.173	0.082	–	–
Fe 4*d*	0	0	0	0	0	0	0.00	10.29
Fe 16*k*	0	0	1, 1.85	0	0	0	1.00	11.35
Fe 16l_1	0	0	0	0	2, 1.67	2, 1.73	0.51	11.34
Fe 16l_2	1, 1.77	0	0	2, 1.83	2, 1.76	2, 1.74	2.72	12.09

[a] The number of hydrogen near-neighbors is given followed by the iron to hydrogen distance, if any, given in Å.
[b] The Wigner–Seitz cell volumes have been calculated [25] by using the 12-coordinate metallic radii of 1.82, 1.26, and 1.44 Å for Nd, Fe, and Ag, respectively, and a covalent radius of 0.32 Å for hydrogen.

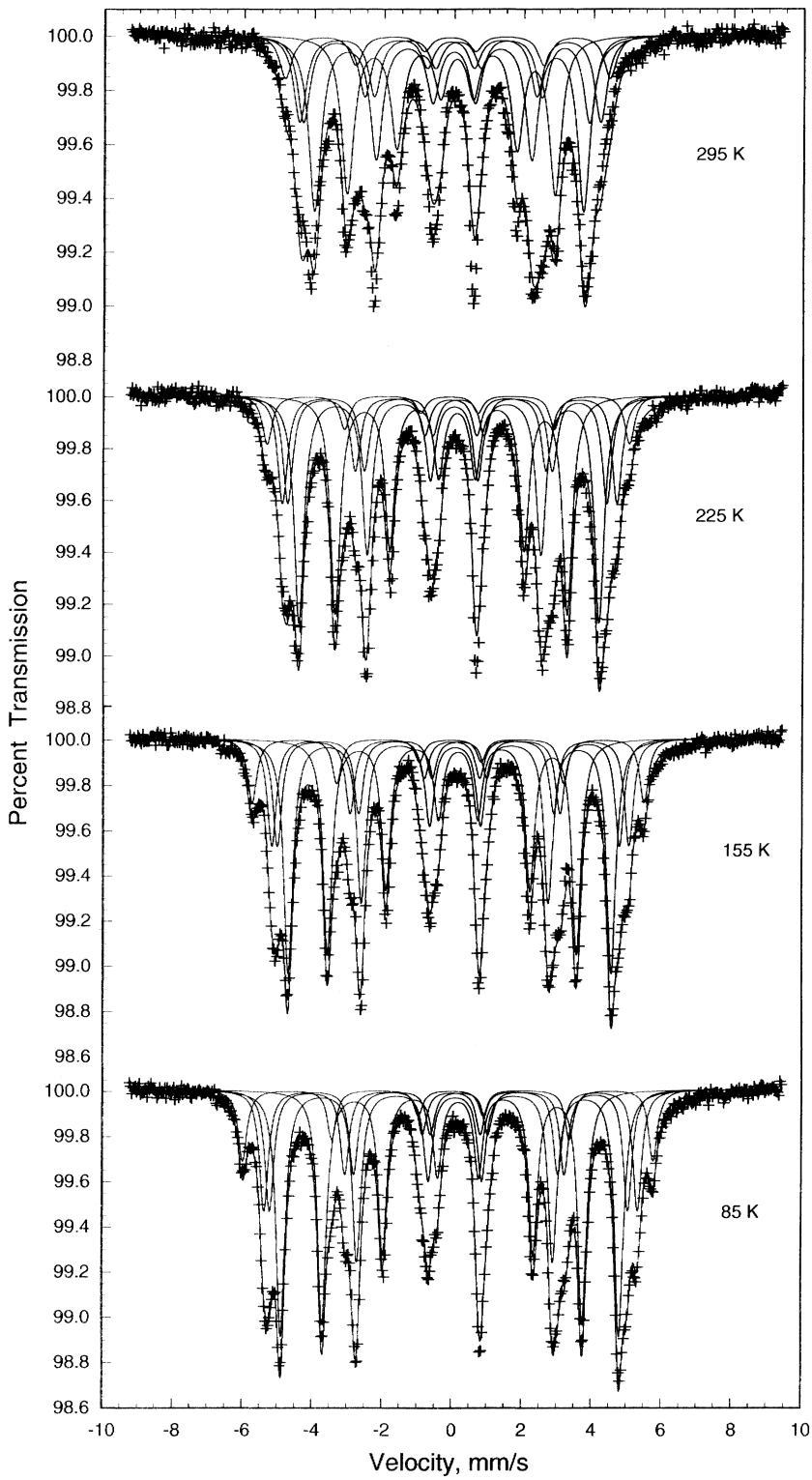

Fig. 1. The Mössbauer spectra of $Nd_6Fe_{13}Ag$ obtained at the indicated temperatures.

of hydrogen has upon the electronic and magnetic properties of $Nd_6Fe_{13}Ag$.

In devising a model to fit the spectra of $Nd_6Fe_{13}Ag$ and $Nd_6Fe_{13}AgH_{13}$ it is useful to refer to the earlier work on related compounds. There have been several earlier Mössbauer studies of $Nd_6Fe_{13}X$, where X is Cu [6], Ag [4,9], Au [4,7], Ge [12], In [13], Tl [13], Sn [9,13], Si [10] and Pb [13]. Depending upon the orientation of the magnetic easy axis, these

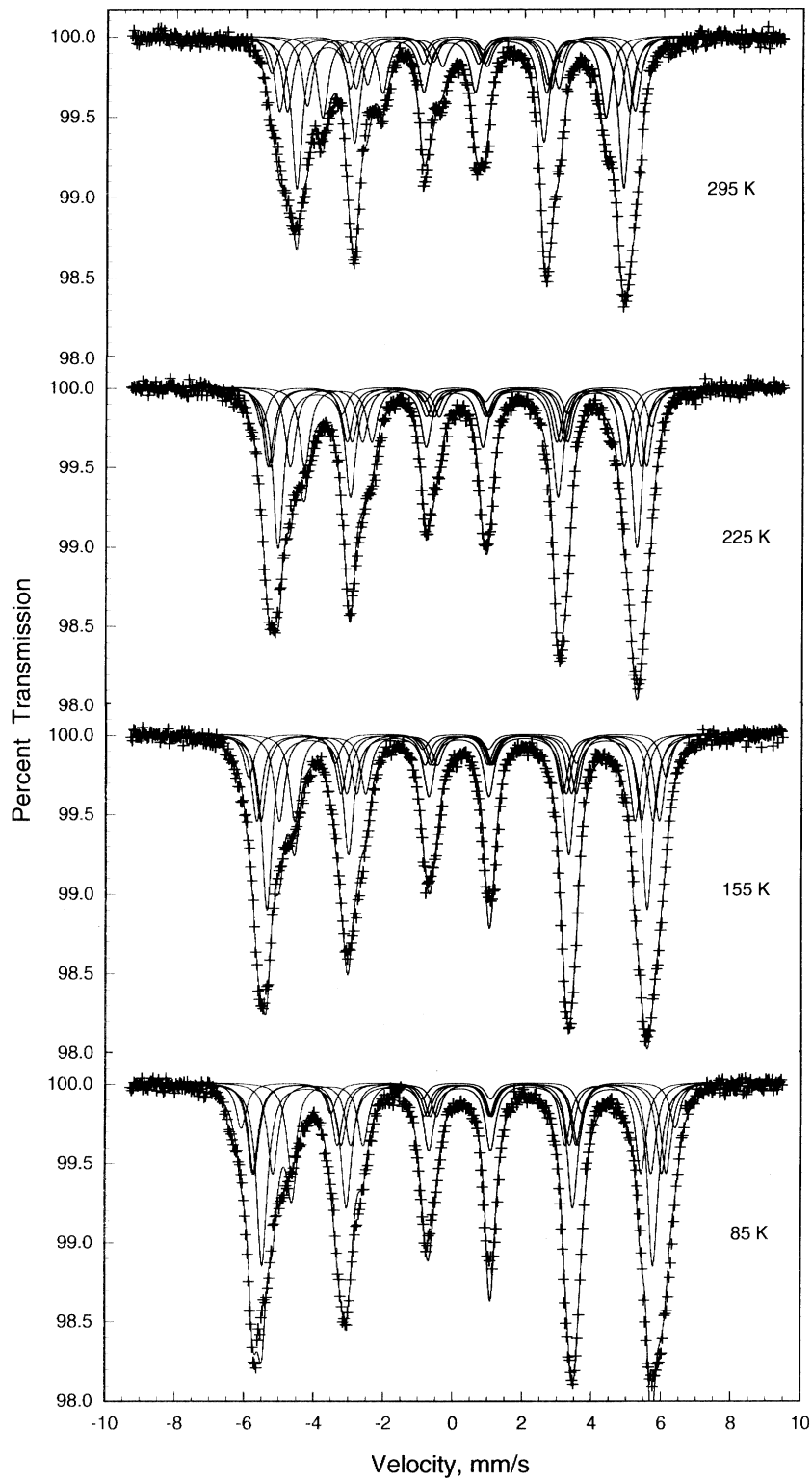

Fig. 2. The Mössbauer spectra of $Nd_6Fe_{13}AgH_{13}$ obtained at the indicated temperatures.

spectra may be analyzed with two quite different models. In the case of a uniaxial *c*-axis magnetization, as is observed [9,13] in $Nd_6Fe_{13}Sn$, the Mössbauer spectra are best fit with four sextets with relative areas in the ratio 4:16:16:16 and assigned to the 4*d*, 16*k*, 16l_1, and 16l_2 crystallographically inequivalent iron sites, respectively. In contrast, in the case of basal magnetization, as is observed in $Nd_6Fe_{13}X$ where X is Ag [4,9], Au [4,7], In [13], Tl [13] and Pb [13], the Mössbauer spectra are best fit with five sextets, with relative areas in the ratio 4:8:8:16:16 assigned to the five, 4*d*, 16*k*, 16*k*′, 16l_1, and

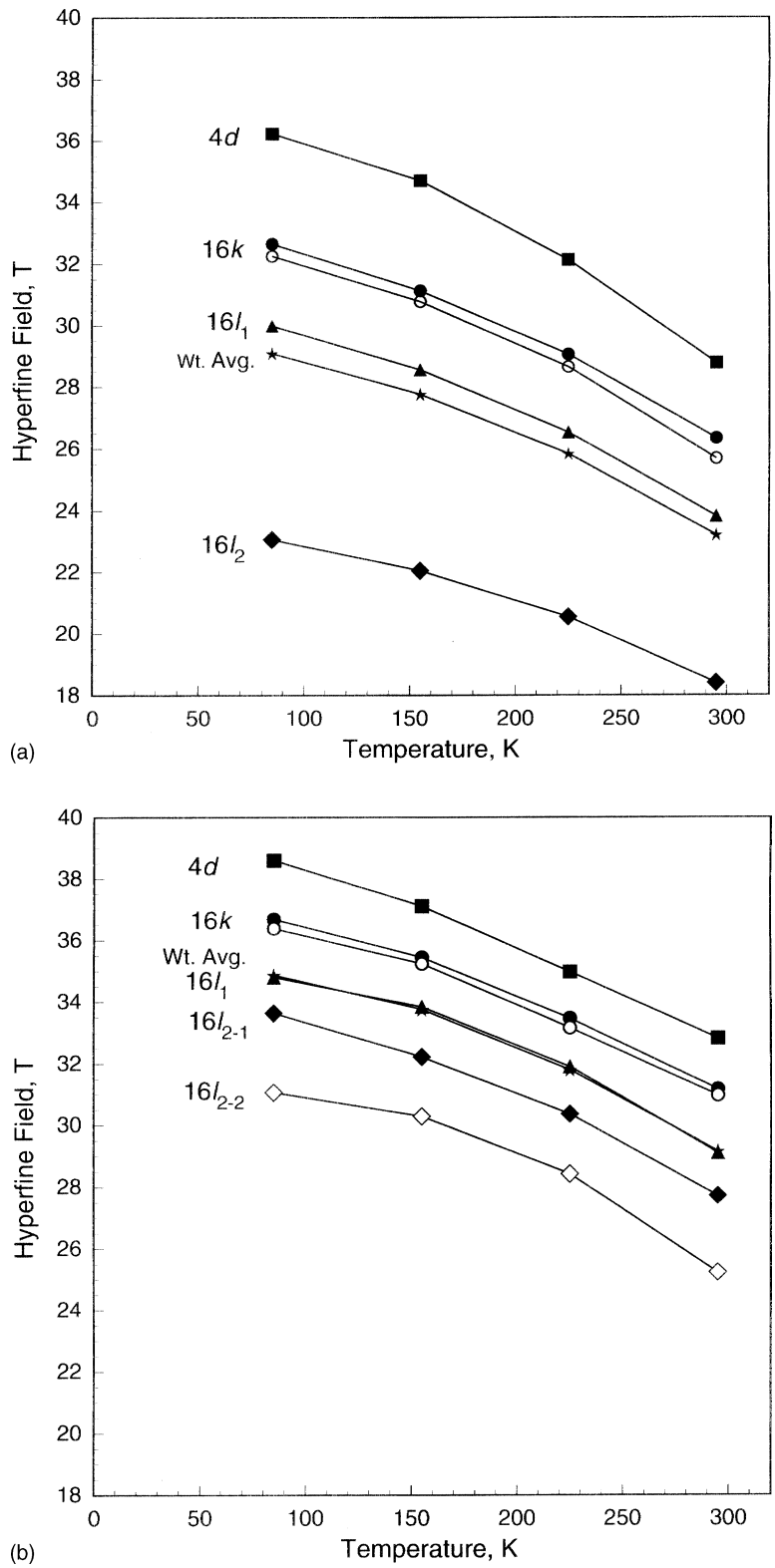

Fig. 3. The temperature dependence of the magnetic hyperfine fields of the four iron sites, and their weighted average, in $Nd_6Fe_{13}Ag$ (a) and $Nd_6Fe_{13}AgH_{13}$ (b). The error bars are approximately the size of the data points.

$16l_2$, crystallographically and magnetically inequivalent iron sites, respectively. Because of both the basal orientation of the magnetization in the latter compounds and the local point symmetry, the dipolar contribution to the magnetic field at the iron 16*k* site removes the magnetic degeneracy of this site and two sextets of equal areas are required in the fits. $Nd_6Fe_{13}Si$ is a special case [10,11] in which a spin reorientation of the magnetic axis below ca. 110 K leads to a dramatic change

Table 3
Mössbauer spectral hyperfine parameters for $Nd_6Fe_{13}Ag$

Parameter	T (K)	4d	16k	16k′	$16l_1$	$16l_2$	Weighted average
H (T)	295	28.8	26.3	25.7	23.8	18.4	23.2
	225	32.1	29.1	28.6	26.5	20.6	25.8
	155	34.7	31.1	30.8	28.6	22.0	27.8
	85	36.2	32.6	32.2	30.0	23.1	29.1
δ (mm/s)[a]	295	−0.161	−0.085	−0.085	−0.079	−0.010	−0.066
	225	−0.128	−0.049	−0.049	−0.047	0.024	−0.032
	155	−0.094	−0.011	−0.011	−0.008	0.067	0.008
	85	−0.062	0.022	0.022	0.025	0.102	0.041

[a] Relative to room temperature α-iron foil.

in the Mössbauer spectra, a change that requires both of the above models for adequate fits.

As reported earlier [8] the magnetization of $Nd_6Fe_{13}Ag$ is basal and, as may be seen in Fig. 1, the Mössbauer spectra are fit excellently with five sextets. In these fits the isomer shifts of the 16*k* and 16*k*′ sites have been constrained to be identical and, in the initial [8] fits of the $Nd_6Fe_{13}Ag$ spectra, the relative areas of the five sextets were constrained to the magnetic degeneracies of the iron sites, i.e., 4:8:8:16:16, and it was assumed that there was no texture in the absorber. In the fits shown in Fig. 1 the influence of texture, which is clearly visible [8] in the large relative areas of the second and fifth lines, has been included as a variable, *x*, in the ratio of the relative component areas, 3:*x*:1:1:*x*:3, in each of the five sextets. Further, because of the possibility of slightly different recoil free fractions for the different iron sites, the relative areas of the five sextets were allowed to vary, with the constraint that the area of the 16*k* and 16*k*′ sextets were equal. In all cases the relaxation of the relative area constraint led to, at most, trivial changes in the relative areas and virtually no changes in the hyperfine parameters. Indeed, for $Nd_6Fe_{13}Ag$ the relative areas of the five sextets depart by at most 3% from the expected crystallographic ratio.

The fits of the $Nd_6Fe_{13}AgH_{13}$ Mössbauer spectra are more complex because of the presence of hydrogen as a near neighbor of some but not all of the iron sites, see Table 2. In view of the number of hydrogen near neighbors one would expect the changes in the hyperfine parameters upon hydrogenation to be the smallest for the iron 4*d* site which has zero hydrogen near neighbor and largest for the iron $16l_2$ site which has on average 2.72 hydrogen near neighbors. The consequence of this large number of hydrogen near neighbors is to substantially broaden the sextet that is associated with the iron $16l_2$ site such that it must be fit with two sextets one of which corresponds to iron sites with fewer hydrogen near neighbors, labeled the $16l_{2-1}$ site, and a second site which corresponds to iron sites with more hydrogen near neighbors, labeled the $16l_{2-2}$ site. The resulting model then consists of six sextets in a ratio 4:8:8:16:8:8 assigned to the six 4*d*, 16*k*, 16*k*′, $16l_1$, $16l_{2-1}$, and $16l_{2-2}$ sites, respectively. Although the isomer shifts for the $16l_{2-1}$ and $16l_{2-2}$ site component sextets are not constrained to be equal, all the remaining constraints used in the fits of the spectra of $Nd_6Fe_{13}Ag$ have been retained in the fits of the spectra of $Nd_6Fe_{13}AgH_{13}$.

The magnetic hyperfine fields observed at 85 and 295 K for the different iron sites in $Nd_6Fe_{13}Ag$ have been reported earlier and found to increase with the number of iron near neighbors for each site. Specifically, in both $Nd_6Fe_{13}Ag$ and $Nd_6Fe_{13}AgH_{13}$ the 4*d*, 16*k*, $16l_1$, and $16l_2$ sites have 12, 10, 9, and 7 iron near neighbors as determined [25] from the Wigner–Seitz cell of each iron site and, as may be seen in Fig. 3, the hyperfine fields decrease in this order in both $Nd_6Fe_{13}Ag$ and $Nd_6Fe_{13}AgH_{13}$. The hyperfine fields obtained at 85 K for $Nd_6Fe_{13}Ag$ are completely compatible with the values reported earlier [4] at 4.2 K and the temperature dependence of the hyperfine fields for both $Nd_6Fe_{13}Ag$ and $Nd_6Fe_{13}AgH_{13}$ show the expected uniform decrease with increasing temperature.

Table 4
Mössbauer spectral hyperfine parameters for $Nd_6Fe_{13}AgH_{13}$

Parameter	T (K)	4d	16k	16k′	$16l_1$	$16l_{2-1}$	$16l_{2-2}$	Weighted average
H (T)	295	32.8	31.2	31.0	29.1	27.7	35.2	29.2
	225	34.9	33.5	33.2	31.9	30.4	28.4	32.0
	155	37.1	35.4	35.2	33.8	32.2	30.3	33.8
	85	38.6	36.7	36.4	34.8	33.6	31.1	34.9
δ (mm/s)[a]	295	−0.013	0.017	0.017	−0.014	0.138	0.261	0.063
	225	0.031	0.080	0.080	0.045	0.191	0.283	0.114
	155	0.075	0.127	0.127	0.121	0.205	0.308	0.161
	85	0.120	0.155	0.155	0.164	0.230	0.352	0.197

[a] Relative to room temperature α-iron foil.

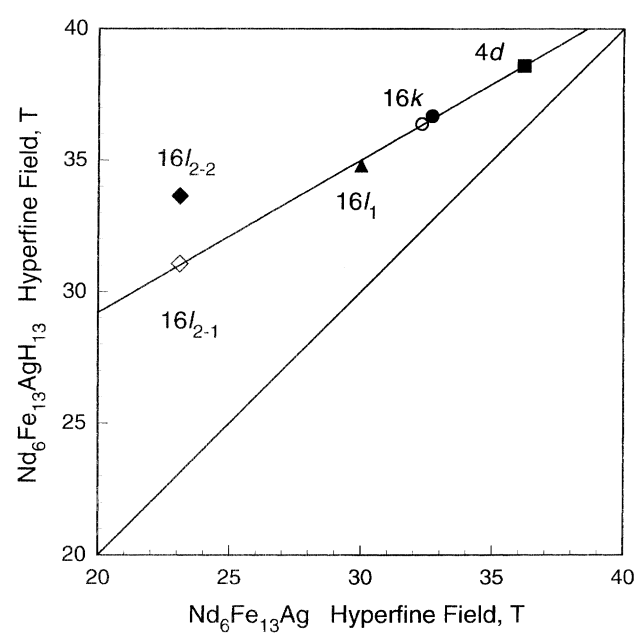

Fig. 4. A comparison of the magnetic hyperfine fields observed at 85 K in $Nd_6Fe_{13}Ag$ and $Nd_6Fe_{13}AgH_{13}$. The $16l_{2-2}$ site has been ignored in the linear fit of the results because this site has the most hydrogen near neighbors. The line of unit slope is also shown and the error bars are approximately the size of the data points.

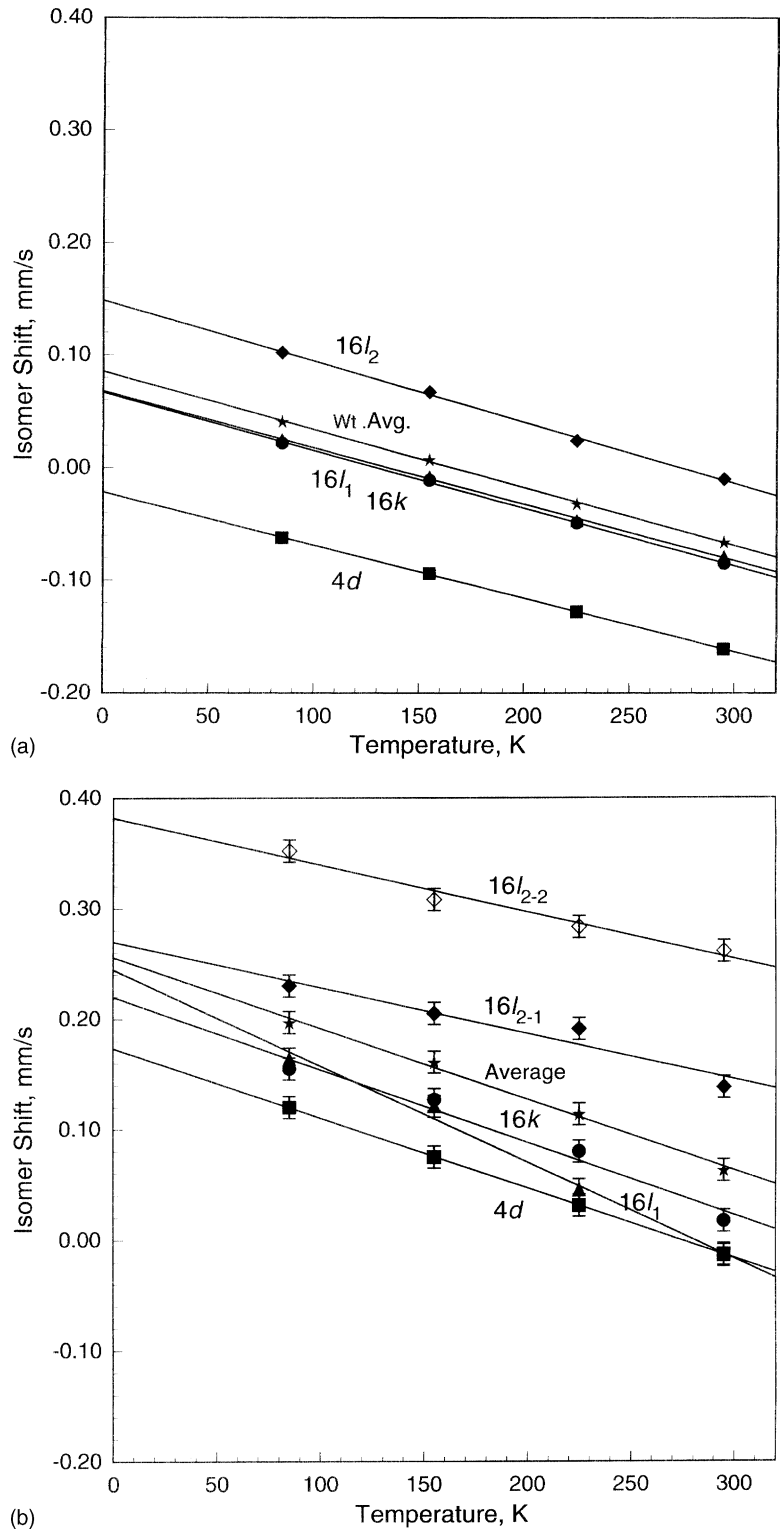

Fig. 5. The temperature dependence of the isomer shifts of the iron sites, and their weighted average, in $Nd_6Fe_{13}Ag$ (a) and $Nd_6Fe_{13}AgH_{13}$ (b).

Perhaps more illustrative of the influence of the hydrogen upon the magnetic properties of $Nd_6Fe_{13}Ag$ upon forming $Nd_6Fe_{13}AgH_{13}$ is the plot, see Fig. 4, of the 85 K hyperfine fields of the different sites observed in $Nd_6Fe_{13}Ag$ as compared with those observed in $Nd_6Fe_{13}AgH_{13}$. This plot clearly shows the importance of the presence of the hydrogen on all the iron sites, for which all of the hyperfine fields have increased substantially. Further, this figure clearly shows that the increase in the hyperfine field is the largest for the $16l_2$ sites, and especially for the $16l_{2-2}$ site, just the

sites that have the largest number of hydrogen near neighbors.

The above assignments of the components observed in the Mössbauer spectra of $Nd_6Fe_{13}Ag$ and $Nd_6Fe_{13}AgH_{13}$ are supported by the isomer shifts observed for each sextet. As may be observed in Fig. 5, for both compounds the isomer shift of each crystallographic iron site decreases, as expected, approximately linearly with increasing temperature. However, in the case of $Nd_6Fe_{13}AgH_{13}$ the isomer shifts of the $16l_{2-1}$ and $16l_{2-2}$ sites are increased dramatically by the presence of the 2.72 hydrogen near neighbors. Further, the isomer shift of the $16l_1$ site which has 0.51 hydrogen near neighbors increases substantially upon cooling whereas the 4*d* site with no hydrogen near neighbors, although increased in value, has a temperature dependent slope that is very similar in both $Nd_6Fe_{13}Ag$ and $Nd_6Fe_{13}AgH_{13}$. Surprisingly, the 16*k* site, which has one hydrogen near neighbor and whose isomer shift is increased substantially, also has a similar slope. A better illustration of the influence of the hydrogen on the isomers shifts in shown in Fig. 6, a plot of the 85 K isomer shifts observed for the different sites in $Nd_6Fe_{13}Ag$ as compared with those observed in $Nd_6Fe_{13}AgH_{13}$. This figure shows both the increase in the isomer shifts of all of the iron sites upon hydrogenation and the dramatic increase in the $16l_{2-1}$ and especially the $16l_{2-2}$ sites because of the presence of the 2.72 hydrogen near neighbors.

A number of studies [10,15–22,26–33] have reported a close to linear correlation between the Mössbauer effect isomer shift with the Wigner–Seitz cell volume of a given iron site in a variety of iron-containing intermetallic compounds. The Wigner–Seitz cell volumes of the four crystallographically inequivalent iron sites in $Nd_6Fe_{13}Ag$ have been calculated [25] and found to be 10.66, 11.51, 11.58, and 12.89 $Å^3$ for the iron 4*d*, 16*k*, $16l_1$, and $16l_2$ sites, respectively; the analogous cell volumes for $Nd_6Fe_{13}AgH_{13}$ are given in Table 2. As is illustrated in Fig. 7, this correlation is also observed in both $Nd_6Fe_{13}Ag$ and $Nd_6Fe_{13}AgH_{13}$. It is immediately obvious from this figure that the presence of hydrogen in $Nd_6Fe_{13}AgH_{13}$ increases all of the isomer shifts partly in response to the associated expansion of the unit cell upon hydrogenation, an expansion which increases the volume available to each iron site, reduces the s-electron density at the iron-57 nucleus and hence increases the isomer shift. However, the added presence of the hydrogen near neighbors, especially at the $16l_2$ sites is obvious.

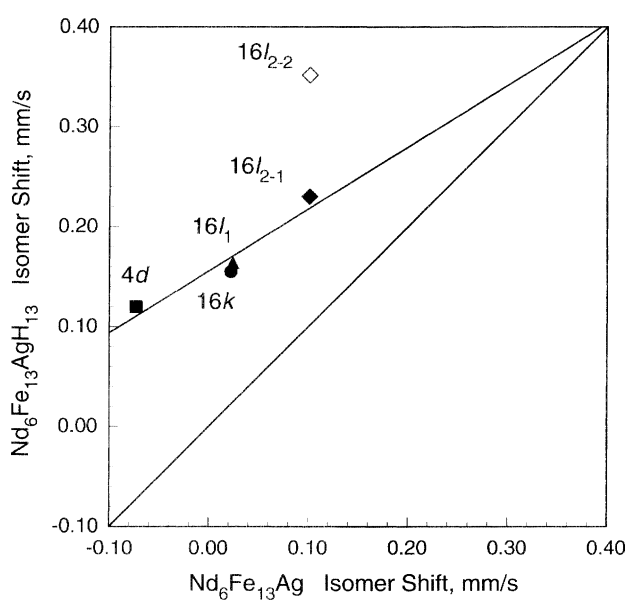

Fig. 6. A comparison of the isomer shifts observed at 85 K in $Nd_6Fe_{13}Ag$ and $Nd_6Fe_{13}AgH_{13}$. The $16l_{2-2}$ site has been ignored in the linear fit of the results because this site has the most hydrogen near-neighbors. The line of unit slope is also shown.

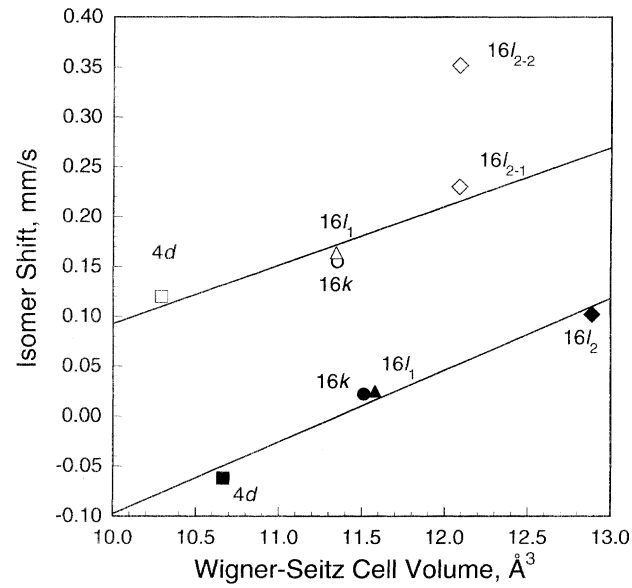

Fig. 7. A plot of the Wigner–Seitz cell volumes vs. the isomer shifts observed at 85 K for $Nd_6Fe_{13}Ag$, solid symbols, and $Nd_6Fe_{13}AgH_{13}$, open symbols. The $16l_{2-2}$ site has been ignored in the linear fit of the results for $Nd_6Fe_{13}AgH_{13}$ because this site has the most hydrogen near neighbors.

4. Conclusions

The Mössbauer spectra of $Nd_6Fe_{13}Ag$ and $Nd_6Fe_{13}AgH_{13}$ obtained between 85 and 295 K can successfully be analyzed with a model which takes into account the basal magnetic anisotropy and the variations in the near-neighbor hydrogen occupancy for each iron site. The assignment of the five sextets in $Nd_6Fe_{13}Ag$ is in complete agreement with the iron near-neighbor environment and the Wigner–Seitz cell volume of the four crystallographically inequivalent iron sites. The assignment of the six sextets in $Nd_6Fe_{13}AgH_{13}$ is in complete agreement with the iron and hydrogen near-neighbor environment and the Wigner–Seitz cell volume of the four crystallographically inequivalent iron sites. Upon hydrogenation, substantial increases in hyperfine field and in the isomer shift are observed for the four crystallographically inequivalent iron sites. These increases are the largest for the $16l_2$

sites, which has the largest number of hydrogen near neighbors. Finally, there is no indication in the Mössbauer spectra observed for $Nd_6Fe_{13}AgH_{13}$ of any dynamic motion of the hydrogen between sites as has been observed [34] in the hydride of Pr_2Fe_{17}.

Acknowledgements

The authors thank Dr. R.P. Hermann for many helpful discussions during the course of this work. The financial support of the University of Liège through grant number 2850006 is acknowledged with thanks. This work was partially supported by the US National Science Foundation through grant INT-9815138.

References

[1] F. Weitzer, P. Rogl, J. Less-Common Met. 167 (1990) 135.
[2] H. Klesnar, P. Rogl, J. Mater. Res. 6 (1991) 53.
[3] J. Allemand, A. Letant, J.M. Moreau, J.P. Nozières, R. Perrier de la Bathie, J. Less-Common Met. 166 (1990) 73.
[4] F. Weitzer, A. Leithe-Jasper, P. Rogl, K. Hiebl, A. Rainbacher, G. Wiesinger, W. Steiner, J. Friedl, F.E. Wagner, J. Appl. Phys. 75 (1994) 7745.
[5] Q.W. Yan, P.L. Zhang, X.D. Sun, B.P. Hu, Y.Z. Wang, X.L. Rao, G.C. Liu, C. Gou, D.F. Chen, Y.F. Cheng, J. Phys. Condens. Matter 6 (1994) 3101.
[6] K.G. Knoch, A. Le Calvez, Q. Qi, A. Leithe-Jasper, J.M.D. Coey, J. Appl. Phys. 73 (1993) 5878.
[7] C.H. de Groot, F.R. de Boer, K.H.J. Buschow, D. Hautot, G.J. Long, F. Grandjean, J. Alloys Compd. 233 (1996) 161.
[8] D. Hautot, G.J. Long, F. Grandjean, C.H. de Groot, K.H.J. Buschow, J. Appl. Phys. 81 (1997) 4535.
[9] G. Wiesinger, A. Rainbacher, W. Steiner, A. Leithe-Jasper, P. Rogl, F. Weitzer, Hyperfine Interact. 94 (1994) 1915.
[10] D. Hautot, G.J. Long, F. Grandjean, C.H. de Groot, K.H.J. Buschow, J. Appl. Phys. 83 (1998) 1554.
[11] O. Isnard, G.J. Long, D. Hautot, K.H.J. Buschow, F. Grandjean, J. Phys. Cond. Matter 14 (2002) 12391.
[12] B.P. Hu, J.M.D. Coey, H. Klesnar, P. Rogl, J. Magn. Magn. Mater. 117 (1992) 225.
[13] F. Weitzer, A. Leithe-Jasper, P. Rogl, K. Hiebl, H. Noël, G. Wiesinger, W. Steiner, J. Solid State Chem. 104 (1993) 368.
[14] G.J. Long, D. Hautot, F. Grandjean, O. Isnard, S. Miraglia, J. Magn. Magn. Mater. 202 (1999) 100.
[15] C. Piquer, F. Grandjean, O. Isnard, G.J. Long, J. Magn. Magn. Mater. 263 (2003) 235.
[16] C. Piquer, F. Grandjean, O. Isnard, G.J. Long, J. Alloys Compd. 353 (2003) 33.
[17] C. Piquer, F. Grandjean, O. Isnard, G.J. Long, J. Appl. Phys. 93 (2003) 3414.
[18] C. Piquer, F. Grandjean, O. Isnard, G.J. Long, J. Magn. Magn. Mater. 265 (2003) 156.
[19] C. Piquer, R.P. Hermann, F. Grandjean, O. Isnard, G.J. Long, J. Phys. Condens. Mater. 15 (2003) 7395.
[20] C. Piquer, F. Grandjean, O. Isnard, V. Pop, G.J. Long, J. Alloys Compd. 377 (2004) 1.
[21] C. Piquer, F. Grandjean, O. Isnard, V. Pop, G.J. Long, J. Appl. Phys. 95 (2004) 6308.
[22] C. Piquer, F. Grandjean, O. Isnard, G.J. Long, J. Alloys Compd., in press.
[23] S.L. Ruby, , in: I.J. Gruverman, C.W. Seidel (Eds.), Mössbauer Effect Methodology, 8, Plenum Press, New York, 1973, p. 263.
[24] V.A. Yartys, F.R. de Boer, K.H.J. Buschow, B. Ouladdiaf, H.W. Brinks, B.C. Hauback, J. Alloys Compd. 356–357 (2003) 142.
[25] L. Gelato, J. Appl. Cryst. 14 (1981) 151.
[26] G.J. Long, O.A. Pringle, F. Grandjean, K.H.J. Buschow, J. Appl. Phys. 72 (1992) 4845.
[27] G.J. Long, O.A. Pringle, F. Grandjean, W.B. Yelon, K.H.J. Buschow, J. Appl. Phys. 74 (1993) 504.
[28] G.J. Long, O.A. Pringle, F. Grandjean, K.H.J. Buschow, J. Appl. Phys. 75 (1994) 2598.
[29] G.J. Long, S. Mishra, O.A. Pringle, F. Grandjean, K.H.J. Buschow, J. Appl. Phys. 75 (1994) 5994.
[30] D.P. Middleton, S.R. Mishra, G.J. Long, O.A. Pringle, Z. Hu, W.B. Yelon, F. Grandjean, K.H.J. Buschow, J. Appl. Phys. 78 (1995) 5568.
[31] G.J. Long, F. Grandjean, J. Magn. Magn. Mater. 162 (1996) 162.
[32] F. Grandjean, D. Hautot, G.J. Long, O. Isnard, S. Miraglia, D. Fruchart, J. Appl. Phys. 85 (1999) 4654.
[33] D. Hautot, G.J. Long, F. Grandjean, O. Isnard, Phys. Rev. B 62 (2000) 11731.
[34] D. Hautot, G.J. Long, F. Grandjean, O. Isnard, S. Miraglia, J. Appl. Phys. 86 (1999) 2200.